Journal of Engineering Science and Technology
Vol. 13, No. 8 (2018) 2520 - 2532

OPTIMAL DESIGN OF EQUIVALENT LINEAR INDUCTION MOTOR BASED ON HARMONY SEARCH ALGORITHM AND ANALYSIS USING FINITE ELEMENT METHOD

CH. V. N. RAJA*, K. RAMA SUDHA

Department of Electrical Engineering, A.U. College of Engineering (A),
Visakhapatnam, 530003, Andhra Pradesh, India
*Corresponding Author: ch.v.n.rajar@gmail.com

Abstract

Linear Induction motors (LIM) are used extensively in industrial applications to develop linear motion, especially in transportation systems. These applications need high efficiency with high power factor. Mainly LIM suffer from two major drawbacks, low power factor and low efficiency. These drawbacks cause high-energy consumption and high input current. In this paper, a novel multi objective Harmony Search optimization algorithm (HSA) is proposed to meet required efficiency and power factor in the design of a Linear Induction Motor. Hence, LIM dimensions can then be optimized by using a HSA in an appropriate objective functions. 2-D Finite Element Method is adopted to analyse the flux density in LIM with the parameters obtained using HSA.

Keywords: FEM analysis, FEMM software, Dynamical model, Harmonic search Algorithm, Linear Induction motor, MATLAB 2013a.

1. Introduction

Linear Induction motor (LIM) is an advanced version of motor that is in use to achieve rectilinear motion instead of rotational motion as in ordinary conventional motors. The stator is cut axially and spread out flat. The LIM is broadly applicable in variety of applications such as military, transportation, actuators, robot base movers elevators, etc., [1] due to easy maintenance, high acceleration/deceleration and no need of transformation system from rotary to translational motion.

Rinkevičienė et al. [2] discussed application of linear induction motor in mechatronic systems. Im et al. [3] describes an optimization problem using the Interior Point algorithm (IPA) to meet desired specifications. Yoon et al. [4], optimization is performed to LIM based on starting thrust and output power to input volt-ampere ratio. Jianzhong et al. [5] developed intelligent simulated annealing (ISA) algorithm program package to meet required torque, efficiency and cost. Wai and Liu [6] developed nonlinear control strategy from lyapunov's principle to control LIM servo drive for periodic motion.

Isfahani et al. [7] proposed a multi-objective genetic algorithm optimization method to improve both motor power factor and efficiency. Also analysed the effect of parameters on power factor and efficiency. Liu et al. [8] discussed on a Neighborhood Topology algorithm (NTA) to maintain high starting thrust and high reliability for high-voltage circuit breaker. Bousserhane et al. [9] intended an Adaptive Backstepping controller for LIM to achieve a position and flux tracking objective under disturbance of load torque and parameter uncertainties. Ravanji and Nasiri-Gheidari [10] proposed multi objective genetic algorithm (GA) to design equivalent single sided LIM for machine tool applications and also analysed the obtained parameter values using a 2-D finite-element method.

Hasirci et al. [11] discussed about design, execution and nonlinear velocity tracking control of a novel maglev system for maglev trains. Shiri and Shoulaie [12] derived analytical expression for braking force of LIM based on iron saturation, transverse edge effect, longitudinal end effect and skin effect. Pourmoosa and Mirsalim [13] introduced ICA to equivalent linear induction motor based on coupled-circuit model.

Cirrincione et al. [14] implemented an adaptive neural network based model reference system (NNMRAS) for low speed LIM drives. Ahmed and Abd [15] suggested indirect field oriented voltage control to improve Linear Induction Motor Performance. Xu et al. [16] implemented sliding mode observer to LIM in order to reduce the steady state error and suppress the integral saturation. Chiang et al. [17] proposed an optimized adaptive tracking control for a LIM drive by considering the uncertainties like friction force, unknown end effects and payload. Zayandehroodi et al. [18] introduced a multi-objective cuckoo optimization algorithm (COA) enhanced to improve both efficiency and power factor.

This paper is organized as follows; Section 2 describes Equivalent Circuit, Section 3 describes Identification of LIM parameters using HSA, Section 4 describes the dynamical model of LIM, Section 5 describes FEM Analysis for LIM and Section 6 describes the computer simulations results.

2. Machine Modelling

Figure 1 shows the architecture of the single sided LIM. It contains a three-phase primary and an aluminium laid sheet on the secondary back iron [7].

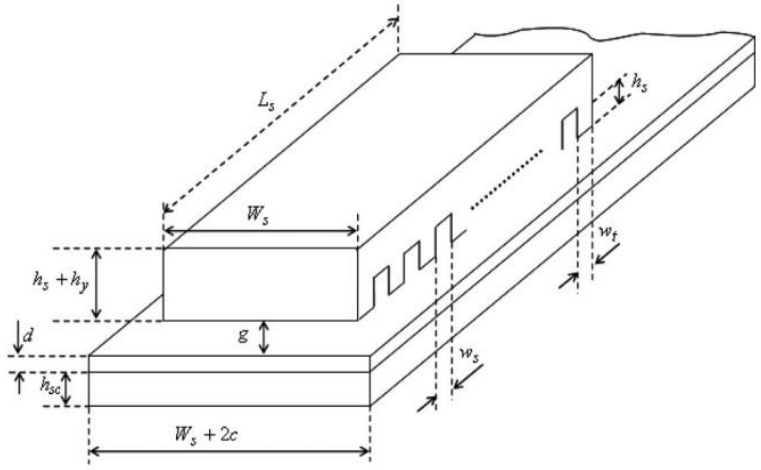

Fig. 1. Architecture of a single sided LIM.

Equivalent Circuit model of LIM

In 1983, Duncan implemented the equivalent circuit model of LIM. The per-phase equivalent circuit model of SLIM is shown in Fig. 2.

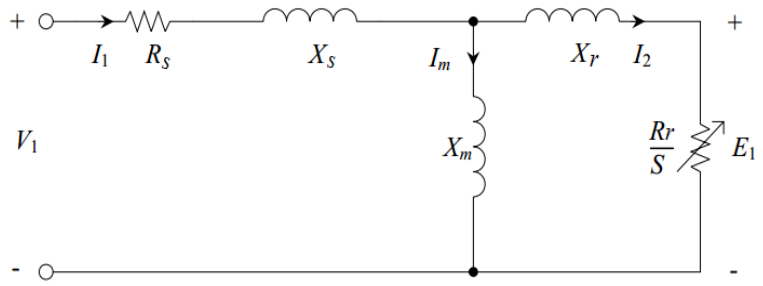

Fig. 2. Equivalent circuit of a LIM.

$$R_s = \frac{\rho_w \, l_w}{A_{wt}} \tag{1}$$

$$X_s = \frac{2\mu_0 \pi \left[\left(\lambda_s \left(1 + \frac{3}{p} \right) + \lambda_d \right) \frac{W_s}{q} + \lambda_e I_{ce} \right] N^2}{p} \tag{2}$$

$$\lambda_s = \frac{h_s(1+3k_p)}{12w_s};\ \lambda_d = \frac{5\left(\frac{g_e}{w_s}\right)}{5+4\left(\frac{g_0}{w_s}\right)}\ \text{and}\ \lambda_e = 0.3(3k_p - 1) \tag{3}$$

$$X_m = \frac{24\,\mu_0\,\pi\pi f_{se} K_w N_1^2 \tau}{\pi^2 p\, g_e} \tag{4}$$

$$R_r = \frac{X_m}{G} \tag{5}$$

$$G = \frac{2\,\mu_0 f_1 \tau^2}{\pi\left(\frac{\rho_r}{d}\right) g_e} \tag{6}$$

$$F_s = \frac{mI_1^2 R_r}{\left[\frac{1}{(sG)^2}+1\right] sV_s} \tag{7}$$

$$\eta = \frac{F_s 2\tau\, f_1(1-s)}{F_s 2\tau\, f_1 + 3I^2 R_1} \tag{8}$$

$$\cos\phi = \frac{F_s 2\tau\, f_1 + 3I^2 R_1}{3VI} \tag{9}$$

Isfahani et al. [7] explained effect of different parameters on efficiency and power factor and hence it is necessary to employ an optimization method to achieve required specifications. Table 1 describes design variables of optimization problems for LIM.

Table 1. Design variables of optimization problem.

Parameter	Max.	Min.
Maximum thrust slip (*s*)	0.1	0.3
Pole Pitch (τ)	40	60
Aluminium thickness	3	6
Primary current Density	1	3
Efficiency (η)	0.7	--
Power Factor	0.7	--

3. Identification of LIM parameters using HSA

In order to improve efficiency and power factor of LIM, the effective design parameters should be known. In this section, the design parameters are chosen as maximum thrust slip, pole pitch, aluminium thickness and primary current density. The design variables and constraints are as listed in Table 1. To obtain required efficiency and power factor the objective function is defined as Eq. (10)

$$f_n(x_1,x_2, x_3,x_4) = \eta(s, \tau, d, J)^{k1}.p_f(s, \tau, d, J)^{k2} \quad (10)$$

As seen in Eq. (15), the power factor and the efficiency are adjusted by power coefficients to meet required performance. Minimization of f_n fulfils both objectives of the optimization. When power factor is more important, choose k_1=0, k_2= 1 and when efficiency is more important than power factor, choose k_1=1, k_2= 0. By considering k_1=k_2= 1, optimized simultaneously to meet desired efficiency and power factor.

Harmony Search Algorithm (HSA) is an optimization algorithm developed by Wang et al. in 2015 [19], Fig. 3. HSA is an advanced process control and optimization for industrial scale systems. HSA is based on the musical process where music players manage the pitches of their instruments to find necessary harmony. Steps involved in the process of HSA are as follows:

i. Assign the number of parameters to be identified for a LIM.

ii. Initialize the HSA parameters such as HM, HMCR, PAR, BW and maximum number of iterations for convergence (shown in Table 2).

iii. Define the multi objective function as

$$\left.\begin{aligned} f_1 &= \eta(s,\tau,d,J) = \eta(x_1,x_2,x_3,x_4) \\ f_2 &= p_f(s,\tau,d,J) = p_f(x_1,x_2,x_3,x_4) \end{aligned}\right\} \quad (11)$$

iv. Defined the range of s, τ, d and J values for the function variables.

v. Obtain functional value of initial Harmony memory.

vi. Set iteration counter t=0.

vii. Increment the iteration counter t=t+1.

viii. Starting of Harmony Search, if generated random value > HMCR.

Then select the value of parameter randomly as,

$$x_{inew} = x_{old} + rand(0,1) * BW \quad (12)$$

Otherwise, choose harmony value from the HM and adjust the pitch as

$$x_{new} = x_{old} + BW * (rand - 0.5) \quad (13)$$

i. Update the HM of objective function and replace the worst solution with new better solution.

ii. Check the stopping criteria and convergence, i.e., number of iteration> maximum iteration, if it is satisfied go to step (xii).

iii. Perform for new Harmony, i.e., increase the iteration count and go to step (vii).

iv. Find the best harmony from the HM, i.e., the optimal values within the constraints.

v. Stop.

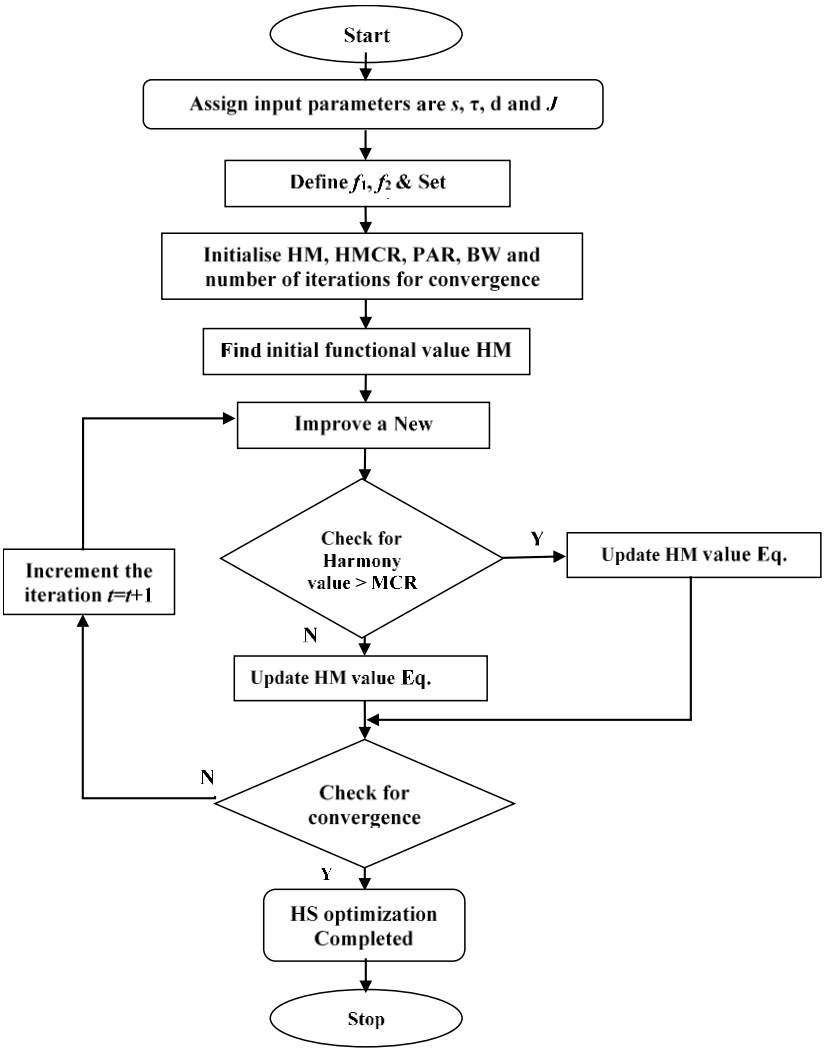

Fig. 3. Flowchart of HSA.

Table 2 describes the parameters of HSA. From Table 3 it is observed that the proposed HSA method shows better results with respect to maximum thrust slip (*s*), pole pitch (τ), aluminium thickness (*d*) and primary current density (*J*).

Table 2. Parameters of harmony search algorithm.

Harmony Memory Size	10
Harmony Memory Acceptance rate	0.9
Pitch Adjustment Rate	0.5
Band Width	randomly

Table 3. Comparison of various optimization results.

Method	*s*	*τ*	*D*	*J*	*η*	*p.f.*	*tc*
IPA [3]	0.13	48.2463	4.9955	2.0154	0.658	0.551	14
ISA [5]	0.1465	48.2200	4.8100	2.1000	0.6685	0.603	9.26
GA [10]	0.1495	48.0000	4.8000	2.1000	0.6795	0.608	8.16
HSA	0.139	40.3998	4.1019	2.1	0.6914	0.698	2.14

4. Dynamical Modelling of LIM

The dynamic model of the LIM is modified from traditional model of a three-phase, Y-connected and can be modelled in the d-q synchronously rotating frame as [9]

$$\frac{di_{ds}}{dt}=\frac{1}{\sigma L_s}\left(-\left(R_s+\left(\frac{L_m}{L_r}\right)^2 R_r\right)i_{ds}+\sigma L_s\frac{\pi}{\tau}v_e i_{qs}+\frac{L_m R_r}{L_r^2}\phi_{dr}+\frac{PL_m\pi}{L_r\tau}\phi_{qr}v_r+V_{ds}\right) \tag{14}$$

$$\frac{di_{qs}}{dt}=\frac{1}{\sigma L_s}\left(-\sigma L_s\frac{\pi}{\tau}v_e i_{ds}-\left(R_s+\left(\frac{L_m}{L_r}\right)^2 R_r\right)i_{qs}-\frac{PL_m\pi}{L_r\tau}\phi_{dr}v_r+\frac{L_m R_r}{L_r^2}\phi_{qr}+V_{qs}\right) \tag{15}$$

$$\frac{d\phi_{dr}}{dt}=\frac{L_m R_r}{L_r}i_{ds}-\frac{R_r}{L_r}\phi_{dr}+\left(\frac{\pi}{\tau}v_e-P\frac{\pi}{\tau}v_r\right)\phi_{qr} \tag{16}$$

$$\frac{d\phi_{qr}}{dt}=\frac{L_m R_r}{L_r}i_{qs}-\left(\frac{\pi}{\tau}v_e-P\frac{\pi}{\tau}v_r\right)\phi_{dr}-\frac{R_r}{L_r}\phi_{qr} \tag{17}$$

$$F_e=K_f\left(\phi_{dr}i_{qs}-\phi_{qr}i_{ds}\right)=M\dot{v}_r+Dv_r+F_L \tag{18}$$

5. Finite Element Analysis for LIM using GA and HSA

In this paper, the design optimizations were carried out based on the analytical model of the machine and presented in Section II. Such as the validity of the design optimizations greatly depends on the accuracy of the model. However, the model is obtained by simplifications such as considering saturation, nonlinearity of materials, etc. Thus, in this section 2-D time stepping FEM are employed to evaluate the new equivalent circuit LIM model.From the equations of the magnetic field with eddy currents can be written as

$$\nabla \text{x}\,(v\nabla \text{x}\,A)=J_o+J \tag{19}$$

$$J_e=-\sigma\left(\frac{\partial A}{\partial t}+grad\,\phi\right) \tag{20}$$

$$\nabla\bullet J_o=0 \tag{21}$$

Commercial computer software (CCS) is one of the most important and efficient software for 2-D FEM analysis and also to obtain numerical and graphical results. The incomplete Cholesky conjugate gradient (ICCG) method used to solve the finite-element equations. . In FEM, using time-stepping analysis the change in levitated position that is based on the current position is called relative moment is measured. The force is produced by a linearly moving magnetic field acting on conductors in the fields are then calculated using local virtual work method.

6. Simulations Results and discussions

The novel optimization HSA has been applied to meet required efficiency and power factor in the design of a Linear Induction Motor are shown in Figs. 4 to 6 and FEA results of LIM has been shown in Figs. 7 to 10.

From Fig. 4, Interior Point algorithm results are worse than remaining optimization methods, Intelligent simulated Annealing optimization have 66.95% with a power factor of 13.86% less than required, Genetic algorithm have 67.9% efficiency but power factor is 13.14% less than the required, but HSA gives 69.04% and also reached required power factor.

From Fig. 5 the HSA has less number of iteration and better pattern search to reach desired optimum values as compared to ISA, GA methods. Figure 6 shows HSA can produce higher speed as compared to other optimization methods.

Figures 7 and 8 show the density of flux distribution and analysis of LIM graphical flux lines representation, respectively. Figures 9 and 10 shows, comparison of flux density and eddy current density (J_e) of LIM. From Figs. 7 and 8, the flux lines are localized in front of the LIM and expand behind the LIM due to velocity effect. Figures 9 and 10 show comparison of flux density and eddy current density (J_e) of LIM using FEM.

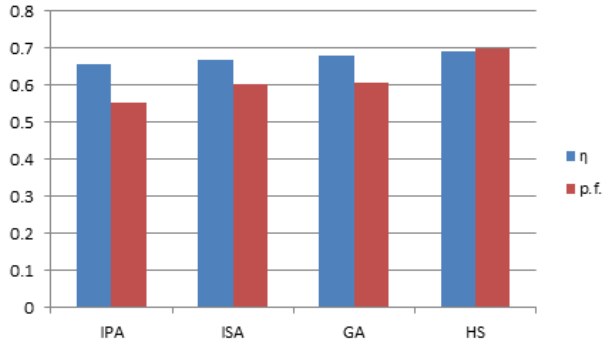

Fig. 4. Comparison of efficiency and power factor between various optimization methods.

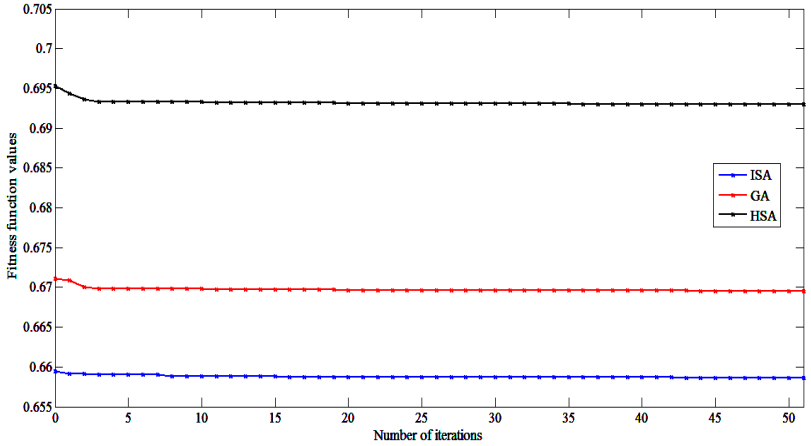

Fig. 5. Comparison Fitness functions of different optimization methods.

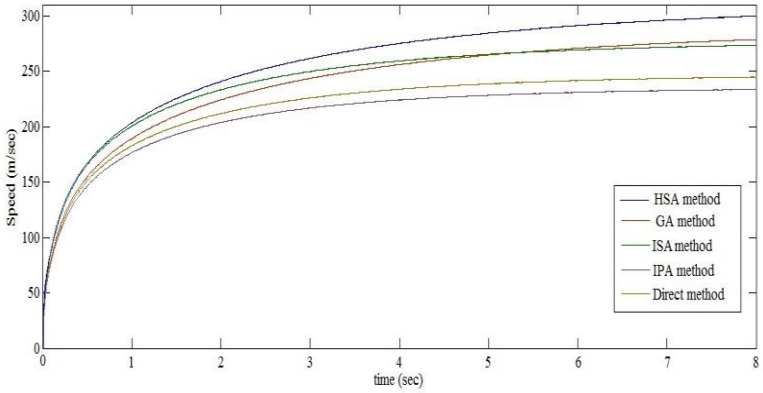

Fig. 6. Comparison of open loop LIM speed for different optimization methods.

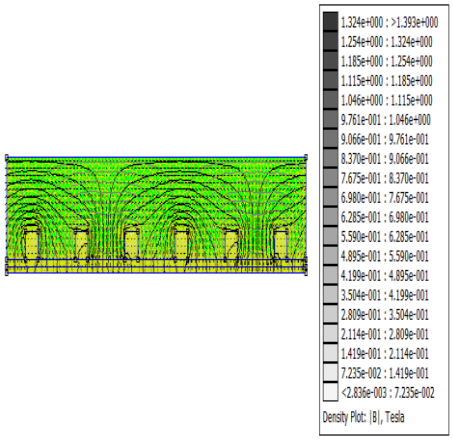

Fig. 7. Flux density distribution in the LIM using HSA.

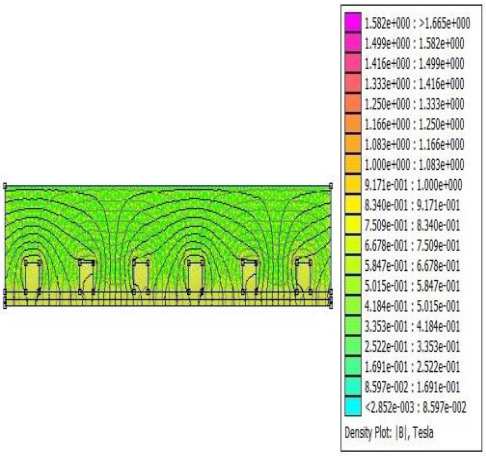

Fig. 8. Flux density distribution in the LIM using GA.

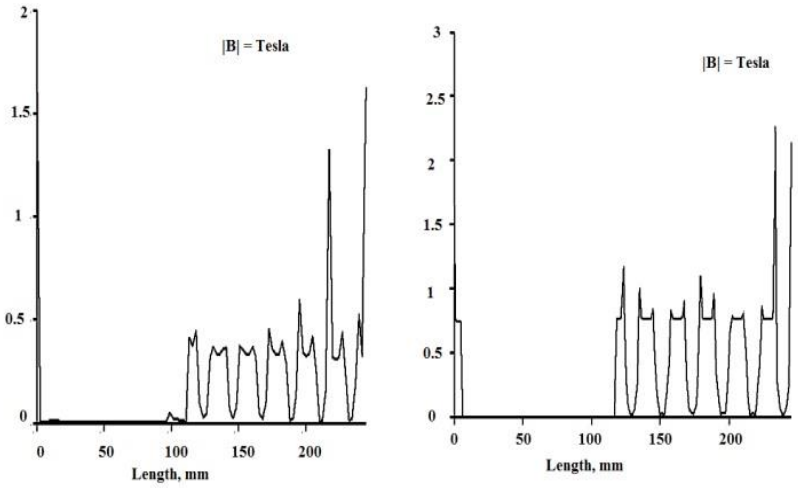

(a) HSA method. **(b) GA method.**

Fig. 9. Comparison Magnitude of flux density in LIM using FEM.

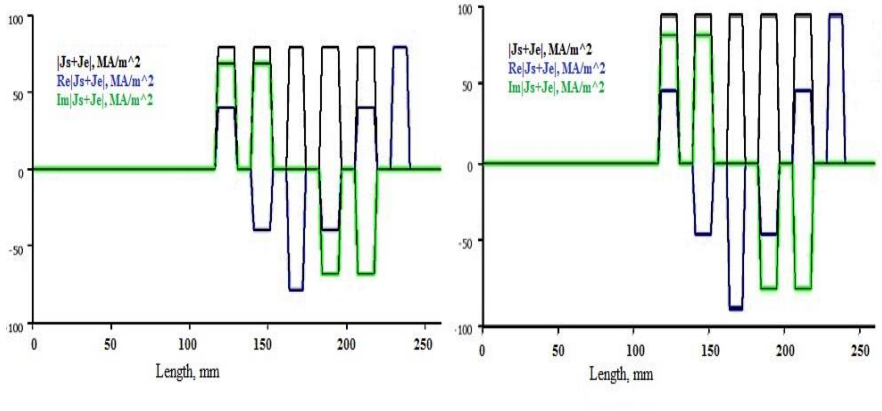

(a) HSA method. **(b) GA method.**

Fig. 10. Eddy current density (J_e) in LIM using FEM.

7. Conclusions

In this paper, multi-objective optimization methods were used for optimized dimensions of a linear induction motor to meet required efficiency and power factor simultaneously. From Table 3, the maximum thrust slip raises the power factor and efficiency. Increase in the primary width to pole pitch ratio leads to an increase in the power factor and a reduction in the efficiency. If the aluminum thickness decreases then efficiency and the power factor values increases. Current density increases the power factor and reduces the efficiency of LIM. From Fig. 4, the usage of intelligent simulated Annealing algorithm have resulted in an efficiency of 66.95% with a power factor of 13.86% less than the required. The GA algorithm yielded an efficiency of 67.9% with a power factor of 13.14% less than the required. The usage of HSA

resulted in an efficiency of 69.14% and also reached the required power factor. From FEMM analysis, HSA based LIM flux and eddy current density is less when compared to GA based LIM, which implies HSA based LIM, consumes less energy and has less input current. Based on the results, we conclude that design of LIM using HSA optimization technique takes less converging time, less number of iterations, desired optimum values to achieve desired efficiency, power factor and high speed.

Nomenclatures

A_{wt}	Cross sectional area of the wire, m^2
D	Viscous friction coefficient
d	Aluminium thickness, m
F_e	Electromagnetic force, N-m
f_l	Primary frequency, Hz
F_L	External force disturbance, N-m
F_s	Thrust force, N-m
G	Goodness factor
g_e	Equivalent air gap, m
i_{ds}	d-axis primary current, Amp
i_{qs}	q-axis primary current, Amp
J	Primary current density, A/m^2
J_e	Eddy current density, A/m^2
k_1	First function constant
k_2	Second function constant
k_p	Pitch factor
k_w	Winding factor
L_m	Magnetizing inductance per phase, Henry
L_r	Secondary inductance per phase, Henry
L_s	Primary inductance per phase, Henry
l_w	Copper wire length per phase, m
M	Total mass of the moving element, Kg
P	Number of pole pairs
R_r	Per-phase rotor resistance, Ohm
R_s	Per-phase stator resistance, Ohm
s	Maximum thrust slip
V_{ds}	d-axis primary voltage, volt
V_{qs}	q-axis primary voltage, volt
v_r	Mover linear velocity, m/s
w_{se}	Equivalent stator width, m
X_m	Magnetizing Reactance per phase, ohm
X_s	Per-phase stator-slot leakage reactance, ohm

Greek Symbols

ϕ	Power factor angle, deg
ϕ_{dr}	Direct axis secondary flux, wb
ϕ_{qr}	Quadratic axis secondary flux, wb
η	Motor efficiency
λ_d	Differential permeance
λ_e	End connection permeance

λ_s	Slot permeance
ρ_r	Volume resistivity of the rotor conductor outer layer, Ω·m
ρ_w	Copper wire volume resistivity, Ω·m
τ	Pole pitch, m

Abbreviations

COA	Cuckoo optimization Algorithm
FEM	Finite Element Method
GA	Genetic Algorithm
HM	Harmony memory
HMCR	Harmony memory considering rate
HSA	Harmony Search Algorithm
ICA	Imperialist competitive Algorithm
IPA	Interior Point Algorithm
ISA	Intelligent simulated Annealing
LIM	Linear Induction Motor
NTA	Neighborhood Topology Algorithm
PAR	Pitch adjusting rate

References

1. Boldea, I.; and Nasar, S.A. (1995). *Linear motion electromagnetic system*. (2nd ed.). New Jersey: John Wiley & Sons Inc.
2. Rinkevičienė, R.; Lisauskas, S.; and Batkauskas, V. (2007). Application and analysis of linear induction motors in mechatronic systems. *4rd International Symposium KURESSAARE 2007*, Kuressaare, Estonia, 69-72.
3. Im D.-H.; Park, S.-C.; and Im, J.-W. (1993). Design of single-sided linear induction motor using the finite element method and SUMT. *IEEE Transactions on Magnetics*, 29(2), 1762-1766.
4. Yoon, S.-B.; Hur, J.; and Huyen, D.-S. (1997). A method of optimal design of single-sided linear induction motor for transit. *IEEE Transactions on Magnetics*, 33(5), 4215-4217.
5. Jianzhong, S.; Fengxian, B.; and Renyuan, T. (2002). Optimization design of special induction motors using improved intelligent simulated annealing algorithm. *ICEMS'2001. Proceedings of the Fifth International Conference on Electrical Machines and Systems (IEEE Cat. No.01EX501)*, China, 1163-1165.
6. Wai, R.-J.; and Liu, W.-K. (2003). Nonlinear control for linear induction motor servo drive. *IEEE Transactions on Industrial Electronics*, 50(5), 920-935.
7. Isfahani, H.A.; Ebrahimi, B.M.; and Lesani H. (2008). Design optimization of a low speed single-sided linear induction motor for improved efficiency and power factor. *IEEE Transactions on Magnetics*, 44(2), 266-272.
8. Liu, A.m.; Zhang, X.l; Lin, X.; and Li Y.-x. (2002). Application of neighbourhood topology particle swarm optimization to cylinder linear induction motor design. *Proceedings of the IEEE conf. on Automation and Logistics*, Shenyang, China, 538-542.
9. Bousserhane, I.K.; Boucheta, A.; Hazzab, A.; Mazari, B.; Rahli, M.; and Fellah M.K. (2009). Adaptive backstepping controller design for linear induction

motor position control. *UPB Scientific Bulletin, Series C: Electrical Engineering*, 71(3), 171-186.

10. Ravanji, M.H.; and Nasiri-Gheidari, Z. (2015). Design optimization of a ladder secondary single-sided linear induction motor for improved performance. *IEEE Transactions on Energy Conversion*, 30(4), 1595 - 1603.
11. Hasirci, U.; Balikci, A.; Zabar, Z.; and Birenbaum, L. (2011). A novel magnetic-levitation system: design, implementation and nonlinear control. *IEEE Transactions on Plasma Science*, 39(1), 492-497.
12. Shiri, A.; and Shoulaie, A. (2012). Design optimization and analysis of single-sided linear induction motor, considering all phenomena. *IEEE Transactions on Energy Conversion*, 27(2), 516-525.
13. Pourmoosa, A.A.; and Mirsalim, M. (2013). Equivalent circuit of linear induction motor based on coupled circuit model and optimization design using imperialist competitive algorithm. *Proceedings of the 4th Annual International Power Electronic & Drive Systems & Technologies Conference*, Tehran, 349-354.
14. Cirrincione, M.; Accetta, A.; Pucci, M.; and Vitale, G. (2013). MRAS speed observer for high-performance linear induction motor drives based on linear neural networks. *IEEE Transactions on Power Electronics*, 28(1), 123-134.
15. Ahmed, A.H.; and Abd, H.Y. (2013). Enhancement of linear induction motor performance using indirect field oriented voltage control. *Engineering and Technology Journal*, 31(12), 2381-2391.
16. Xu, Q.; Cui, S.; Zhang, Q.; Song, L.; and Xiyuan, Li. (2014). Sensorless control research for linear induction motor based on sliding mode observer in electromagnetic aircraft launch system. *Proceedings of the 17th International Symposium on Electromagnetic Launch Technology*, La Jolla, CA, 1-7.
17. Chiang, H.-H.; Hsu, K.-C.; and Li, I.-H. (2015). Optimized adaptive motion control through an SoPC implementation for linear induction motor drives. *IEEE/ASME Transactions on Mechatronics*, 20(1), 348-360.
18. Zayandehroodi, H.; Nasrabadian, A.; and Anoosheh, R. (2015). Cuckoo optimization algorithm based design for low-speed linear induction motor. *Cumhuriyet University Faculty of Science, Science Journal (CSJ)*, 36(6), 29-38.
19. Wang, X.; Gao, X.-Z.; and Zenger, K. (2015). *An introduction to harmony search optimization method*. Poland: Springer International Publishing.